Available online at www.sciencedirect.com

SCIENCE DIRECT®

Journal of Sound and Vibration 280 (2005) 141–157

JOURNAL OF SOUND AND VIBRATION

www.elsevier.com/locate/jsvi

A horizontal fluid-conveying cantilever: spatial coherent structures, beam modes and jumps in stability diagram

M.P. Païdoussis*, A. Sarkar, C. Semler

Department of Mechanical Engineering, McGill University, 817 Sherbrooke Street West, Montreal, Que., Canada H3A 2K6

Received 31 July 2002; accepted 2 December 2003

Abstract

The proper orthogonal decomposition method is used to obtain a low-dimensional model for the planar non-linear dynamics of a horizontal fluid-conveying cantilever undergoing a limit cycle oscillation. The finite-dimensional approximation of the non-linear partial differential equation (PDE) describing the oscillation is carried out by a Galerkin projection scheme, using both the cantilever beam modes and proper orthogonal modes (coherent structures) as projection bases, which leads to a finite set of coupled ordinary differential equations. The proper orthogonal modes are obtained semi-analytically using the cantilever beam modes as a basis. A systematic study is then carried out, focusing on the *jumps* in the linear stability diagram of a horizontal fluid-conveying cantilever vis-à-vis the order of the finite-dimensional model obtained using either the beam modes or the proper orthogonal modes. Depending on the mass-ratio of the cantilever, while the order of the finite-dimensional model using the beam-mode basis increases steadily (up to 10), the corresponding order when the proper orthogonal modes are used to span the solution of the PDE remains unaltered (only two).

1. Introduction

The linear dynamics of a cantilevered pipe conveying fluid is a classical problem of a gyroscopic non-conservative system [1]. The system displays flutter instability by undergoing a Hopf bifurcation resulting in limit-cycle oscillation [1–3]. In order to understand the non-linear behaviour of the system, a consistent non-linear equation of motion accounting for the non-linearity in the stiffness, inertia and damping terms, correct to third order was derived [4]. Theoretical analyses of different variants of the system were carried out [1–5]. The analysis using

---

*Corresponding author. Fax: +1-514-398-7365.

E-mail address: mary.fiorilli@mcgill.ca (M.P. Païdoussis).

0022-460X/$ - see front matter © 2003 Elsevier Ltd. All rights reserved.
doi:10.1016/j.jsv.2003.12.026

Galerkin projections with the beam modes as basis functions was restricted to low-dimensional models only.

This paper continues the recent investigation [6,7] of the authors in order to obtain low-dimensional models for the non-linear dynamics of a cantilever tube conveying fluid and undergoing limit cycle oscillation in the post-flutter region. A Galerkin projection scheme with the linear structural beam modes (also known as Fourier modes) as a basis is used to study a higher-dimensional non-linear dynamical model of a fluid-conveying cantilever. The convergence of the solution scheme of the non-linear PDE in relation to the number of terms retained in the truncated series expansion is systematically studied. Subsequently, attention is focused on the transition of the spatial coherent structures in the stability diagram of the pipe with respect to the mass ratio of the fluid and pipe, in particular in the neighbourhood of the jumps as discussed in Refs. [1,8]. It emerges that while only two dominant proper orthogonal modes can consistently reproduce the dynamics of the PDE, increasingly higher number of beam modes becomes necessary for higher mass ratio to capture the corresponding behaviour.

2. Mathematical model

The schematic diagram of the cantilever pipe under consideration is shown in Fig. 1. The system consists of a tubular beam (pipe) of length L, internal cross-sectional area A, mass per unit length m, flexural rigidity EI, and coefficient of Kelvin–Voigt damping a, conveying fluid of mass M per unit length, with an axial velocity U. The pipe, initially assumed to lie along the x-axis in the direction of gravity, undergoes oscillation $y(s,t)$ in the (x,y) plane, where s is the curvilinear co-ordinate. The centre-line of the pipe is assumed to be inextensible. Introducing the non-dimensional quantities [1,4]

$$\xi=\frac{s}{L},\quad \eta=\frac{y}{L},\quad \tau=\left(\frac{EI}{m+M}\right)^{1/2}\frac{t}{L^2},\quad \alpha=\left(\frac{EI}{m+M}\right)^{1/2}\frac{a}{L^2},$$
$$u=\left(\frac{M}{EI}\right)^{1/2}UL,\quad \gamma=\frac{m+M}{EI}L^3g,\quad \beta=\frac{M}{m+M},\tag{1}$$

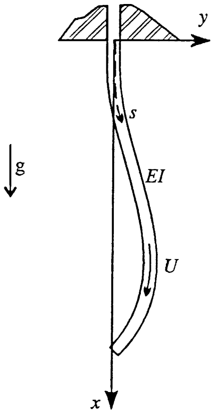

Fig. 1. Schematic of the system.

the equation of motion can be expressed in the following non-dimensional form:

$$\begin{aligned}
&\alpha\dot{\eta}'''' + \eta'''' + \ddot{\eta} + 2u\sqrt{\beta}\dot{\eta}'(1+\eta'^2) + \eta''\Big[u^2(1+\eta'^2) + (\dot{u}\sqrt{\beta}-\gamma)(1-\xi)\Big(1+\tfrac{3}{2}\eta'^2\Big)\Big] \\
&\quad + \gamma\eta'\Big(1+\tfrac{1}{2}\eta'^2\Big) + \Big(1+\alpha\frac{\partial}{\partial t}\Big)[\eta''''\eta'^2 + 4\eta'\eta''\eta''' + \eta''^3] + \eta'\int_0^\xi (\dot{\eta}'^2 + \eta'\ddot{\eta}')\,\mathrm{d}\xi \\
&\quad - \eta''\Big[\int_\xi^1\int_0^\xi (\dot{\eta}'^2 + \eta'\ddot{\eta}')\,\mathrm{d}\xi\,\mathrm{d}\xi + \int_\xi^1 \Big(\tfrac{1}{2}\dot{u}\sqrt{\beta}\eta'^2 + 2u\sqrt{\beta}\eta'\dot{\eta}' + u^2\eta'\eta''\Big)\,\mathrm{d}\xi\Big] = 0. \qquad (2)
\end{aligned}$$

In physical terms, u is the non-dimensional fluid velocity, γ represents the relative measure of gravity to flexural forces, β is the ratio of the fluid mass to the total mass per unit length, and α is the viscoelastic dissipation coefficient; the dot and prime denote derivatives with respect to the non-dimensional time τ and the non-dimensional curvilinear co-ordinate ξ, respectively.

The boundary conditions require the bending moment and shear force at the free end to be zero, and likewise the displacement and slope at the clamped end, i.e., as shown in Ref. [4],

$$\eta(0) = \eta'(0) = \eta''(1) = \eta'''(1) = 0. \qquad (3)$$

Thus, the boundary conditions with flowing fluid are identical to those for a "dry" cantilever.

3. Finite-dimensional representation

An analytical solution of the response field $\eta(\xi,\tau)$ is impossible to obtain. Consequently, a finite-dimensional approximation of the solution is adopted by projecting $\eta(\xi,\tau)$ onto a time-independent global basis which is given by a denumerable and complete set of orthogonal functions in the solution space. One such basis consists of the eigenfunctions of a suitably chosen linear self-adjoint differential operator which depends on the spatial domain and the boundary conditions, e.g., in this case the cantilever beam eigenfunctions. The projection of the non-linear PDE using the Galerkin approach onto these truncated basis functions leads to a finite set of coupled non-linear ODEs which can capture the essential dynamics of the PDE with sufficient accuracy in the regime of interest. However, the number of functions necessary in such a Galerkin projection scheme to reproduce the original system behaviour crucially depends on the appropriate choice of the basis functions. Generally, the basis functions are the normal modes of the linear self-adjoint differential operator corresponding closely to the original non-linear PDE. A Galerkin procedure employing any such set of basis functions $\psi_i(\xi)$ approximates the non-linear PDE (having an infinite number of degrees of freedom) into a finite set of coupled ODEs, with the solution of the original PDE in Eq. (2) being expressed as

$$\eta(\xi,\tau) = \sum_{i=1}^{N} \psi_i(\xi)q_i(\tau), \qquad (4)$$

where the $\psi_i(\xi)$ are the in vacuo cantilever beam eigenfunctions. Performing Galerkin projections, the coupled ODEs corresponding to Eq. (2) are expressed as

$$\ddot{q}_i + C_{ij}\dot{q}_j + K_{ij}q_j + \alpha_{ijkl}q_jq_kq_l + \beta_{ijkl}q_jq_k\dot{q}_l + \gamma_{ijkl}(q_j\dot{q}_k\dot{q}_l + q_jq_k\ddot{q}_l) = 0. \qquad (5)$$

Assuming a steady flow ($\dot{u} = 0$), we obtain

$$C_{ij} = \alpha a_{ij} + 2\sqrt{\beta} u b_{ij}, \quad K_{ij} = a_{ij} + (u^2 - \gamma)c_{ij} + \gamma(d_{ij} + b_{ij}), \tag{6}$$

$$a_{ij} = \int_0^1 \psi_i \psi_j'''' \,\mathrm{d}\xi, \quad b_{ij} = \int_0^1 \psi_i \psi_j' \,\mathrm{d}\xi, \quad c_{ij} = \int_0^1 \psi_i \psi_j'' \,\mathrm{d}\xi, \quad d_{ij} = \int_0^1 \xi \psi_i \psi_j'' \,\mathrm{d}\xi, \tag{7}$$

$$\begin{aligned} \alpha_{ijkl} = {} & \int_0^1 \psi_i (\psi_i'''' \psi_k' \psi_l' + 4\psi_j' \psi_k'' \psi_l''' + \psi_j'' \psi_k'' \psi_l'') \,\mathrm{d}\xi \\ & + u^2 \int_0^1 \psi_i \psi_j'' \left(\psi_k' \psi_l' - \int_\xi^1 \psi_k' \psi_l'' \,\mathrm{d}\xi \right) \mathrm{d}\xi \\ & + \gamma \int_0^1 \psi_i \left(\tfrac{1}{2} \psi_j' \psi_k' \psi_l' - \tfrac{3}{2}(1 - \xi) \psi_j'' \psi_k' \psi_l' \right) \mathrm{d}\xi, \end{aligned} \tag{8}$$

$$\beta_{ijkl} = 2u\sqrt{\beta} \int_0^1 \psi_i \left(\psi_j' \psi_k' \psi_l' - \psi_j'' \int_\xi^1 \psi_k' \psi_l' \,\mathrm{d}\xi \right) \mathrm{d}\xi, \tag{9}$$

$$\gamma_{ijkl} = \int_0^1 \psi_i \psi_j' \left(\int_0^\xi \psi_k' \psi_l' \,\mathrm{d}\xi \right) \mathrm{d}\xi - \int_0^1 \psi_i \psi_j'' \left(\int_\xi^1 \int_0^\xi \psi_k' \psi_l' \,\mathrm{d}\xi \right) \mathrm{d}\xi. \tag{10}$$

In most of the work performed heretofore on this specific system, the cantilever beam modes are used as a basis for the finite-dimensional approximation of the solution. Unfortunately, while the choice of the cantilever beam modes as basis function may constitute an efficient finite representation of a *linear* operator, the existence of non-linearities and flow effects in the PDE generally undermines the efficacy of such a projection basis. Consequently, this approach leads to a relatively high-dimensional representation of the non-linear PDE describing the dynamics of the fluid-conveying cantilever. In the first instance, however, such an approach is adopted here to solve the PDE, and convergence of the solution is studied in relation to the number of terms retained in the expansion. This methodology will be referred to as the Fourier–Galerkin scheme in what follows. The linear stability analysis can be carried out by studying the eigenvalues of the linear system corresponding to non-linear ODEs,

$$\ddot{q}_i + C_{ij} \dot{q}_j + K_{ij} q_j = 0. \tag{11}$$

The onset of oscillatory instability or *flutter*, as exhibited by this specific system, is identified when the imaginary part of any one of the complex eigenfrequencies becomes negative, inducing a negative damping in the system.

4. Proper orthogonal modes: a semi-analytical solution

The dynamics of PDEs are often confined to attractor sets of relatively low dimension when the solution co-ordinates are appropriately chosen. As mentioned before, the cantilever beam eigenfunctions used as basis functions in the Fourier–Galerkin scheme do not contain any information on any of the non-linear or flow-related aspects of the dynamics. Furthermore, by using the cantilever beam eigenfunctions, even linear effects of flow velocity are not taken into account in the basis functions. Thus, the order of the system of ODEs obtained using the Fourier–Galerkin approach is generally considerably larger than the intrinsic dimensionality of the original PDE in certain regions of the parametric space. A logical question is then raised as to how to incorporate the flow and non-linear features existing in the system in order to construct the basis functions and to arrive at a low-dimensional model reflecting the true dimensionality of the original PDE.

The proper orthogonal decomposition method appears to be an obvious choice. The dimensionality and spatio-temporal complexities have successfully been studied using the proper orthogonal decomposition method (PODM) for a wide variety of problems, e.g., Refs. [9–16]. The method "optimally" extracts spatial information and identifies the dimensionality of a system from a set of time-series data gathered from numerical simulations or physical experiments.[1]

The model reduction of the system is carried out next. Firstly, the traditional Fourier–Galerkin scheme is used to obtain the converged solution of the original PDE. Secondly, an efficient POD basis is constructed using the system response from the Fourier–Galerkin scheme, onto which the original PDE is projected to obtain an alternative reduced order model [6,7].

We now briefly describe the PODM for the sake of completeness of the paper. The PODM represents the time series $u(\mathbf{x}, t)$ with an optimal (in the mean-square sense) number of degrees of freedom, where the basis vectors are obtained by solving the mean-square maximization problem [9–16]

$$\lambda = \frac{\int\int_\Omega \langle u(\mathbf{x}, t), u(\mathbf{y}, t)\rangle \Psi(\mathbf{x})\Psi(\mathbf{y})\,\mathrm{d}\mathbf{x}\,\mathrm{d}\mathbf{y}}{\int_\Omega \Psi(\mathbf{x})\Psi(\mathbf{x})\,\mathrm{d}\mathbf{x}}, \tag{12}$$

$\langle . \rangle$ being the time-averaging operator and Ω is the spatial domain of integration. The optimization problem finally yields an eigenvalue problem, stated as

$$\boldsymbol{C}\boldsymbol{\Psi} = \lambda\boldsymbol{\Psi}, \tag{13}$$

where the time-averaged two-point correlation matrix is

$$C_{ij} = \langle u(\mathbf{x}_i, t)u(\mathbf{x}_j, t)\rangle, \tag{14}$$

with $\boldsymbol{\Psi}$ being a typical *spatial coherent structure* in the spatio-temporal records. The dominant eigensubspace of the eigenvalue problem of the correlation matrix, determines the *dominant spatially coherent* modes. An eigenvector $\boldsymbol{\Psi}$ is referred to as the dominant coherent fluctuation or proper orthogonal mode (POM), and λ represents the amount of energy captured by the corresponding mode. The correlation matrix being symmetric and positive-definite, the POMs form a complete orthogonal basis which can represent the process $u(\mathbf{x}, t)$. They are also optimal,[2] in the sense that they capture more energy than any other set of basis functions, with a minimum number of terms. The optimal system dimension N is determined as $\sum_{i=1}^{N}\lambda_i/\sum_{i=1}^{n}\lambda_i \geqslant 99\%$, where n is the order of the $\mathbf{C}$ matrix in Eq. (13) assuming the sufficiency of the POMs to capture 99 percent of the energy of the signal.

---

[1] Here the process is optimal in the mean-square sense. Moreover, there is no guarantee that the method *always* works *well*. Cases where it does not automatically perform satisfactorily have been discussed in Refs. [14,17], for example.

[2] Here "optimality" is strictly in the least-squares sense of capturing most (in this case 99%) of the variance. As pointed out by one of the referees, this does not necessarily mean that the reduced order model itself is optimal or even necessarily correct (as discussed by Cusumano and Lin [18], for example).

In relation to the present study, the solution $\eta(\xi, \tau)$ of the PDE given by Eq. (2) will be approximated using a Galerkin scheme with the POMs as basis, so as to arrive at an optimal low-dimensional model of the attractor set. This approach will be referred to as POD-Galerkin scheme in what follows.

The matrix eigenvalue problem stated in Eq. (13) may have large dimension depending on the system characteristics and vibration response. A significant error can occur in the numerical computation while solving such a large-scale eigenvalue problem. The numerical error occurring in the process is propagated, or even magnified, while performing the differential or integral operation on the numerically generated eigenvectors, as essentially required to derive the discretized equation of motion using the Galerkin projection.

To circumvent the aforementioned limitations, a Galerkin projection scheme [6,7], in addition to approximating the solution of the PDE, is adopted to solve the integral equation in Eq. (13). In this approach, the proper orthogonal modes are projected on the cantilever beam modes as

$$\Psi(\xi) = \sum_{i=1}^{N} \alpha_i \psi_i(\xi). \tag{15}$$

Using the orthogonal properties of the beam modes, the Galerkin error minimization approach leads to the following matrix eigenvalue problem:

$$\boldsymbol{A\alpha} = \lambda \boldsymbol{\alpha}, \tag{16}$$

where

$$A_{ij} = \langle \tilde{q}_i(\tau) \tilde{q}_j(\tau) \rangle. \tag{17}$$

Here $\tilde{q}_i = (q_i - \overline{q_i})$ is the zero-mean response of ith generalized co-ordinate, with $\overline{q_i}$ being its mean. Note that the spatial dependency is removed from the eigenvalue problem in Eq. (6) through the use of the orthonormal properties of the linear cantilever eigenmodes. The typical element A_{ij} in fact represents the correlation between the generalized co-ordinates q_i and q_j. In the present context, the correlations among various generalized co-ordinates incorporate non-linear effects as well as the effects of flow and gravity, including asymmetric gyroscopic features. Evidently, the dimension of the reduced matrix-eigenvalue problem is much smaller in comparison to its full-scale counterpart in Eq. (13); hence, numerical pollution of the eigenvectors is reduced in relation to the full-scale eigenvalue problem.[3] As mentioned before, the approach permits analytical manipulations on the POMs which can be performed on the beam modes. When the POMs are projected on the beam modes, the relative contributions of each beam mode in a dominant POM also reflect the strength of flow and non-linear effects in the system.

5. A horizontal cantilever: jumps on the linear stability plot

Based on the aforementioned mathematical formulation, a numerical investigation is carried out in this section for a fluid-conveying *horizontal* cantilever ($\gamma = 0$) exploring the possibility of

---

[3] For this particular problem, the total number of nodes [in the sense of Fig. 3(b), for instance] is not too large, and hence numerical pollution effects would be minimal; for larger problems, however, the approach adopted could improve the performance of the PODM significantly by reducing numerical pollution in the POMs.

arriving at a reduced model of limit-cycle oscillation (LCO). The results of the linear analysis have already been published [1]. The solutions of the set of non-linear ODEs are obtained by a finite difference method based on Houbolt's scheme [19], with a time-step size of 0.0001.

Fig. 2 shows the stability diagram constructed with a progressively higher number of modes in the Fourier–Galerkin discretization [1,8]. Notice that not only does one not get the first 'jump' with $N = 2$ and does so with $N = 3$ or higher, but also $N = 4$ is required to obtain the second jump, $N = 5$ to obtain the third one, and so on! Clearly, each jump is associated with activation of another generalized co-ordinate, while the approximation prior to the jump is quite reasonable without it [8].

In Fig. 3, the results corresponding to the case of the flow velocity $u = 6.68$ for a fluid-conveying cantilever with $\beta = 0.22$ and $\alpha = 0$ is presented. The eigenvalue distribution of the reduced matrix eigenvalue problem [see, Eq. (16)] is plotted in Fig. 3(a) with $N = 10$. It is seen that there are two dominant eigenvalues, indicating the fact that 2-d.o.f. POD-Galerkin scheme can capture the essential dynamical behaviour of 10-d.o.f. Fourier–Galerkin model. The spatial profiles of these dominant POMs are plotted in Fig. 3(b) along with the corresponding linear normal modes. Figs. 3(c) and (d) show the bar chart of the first two eigenvectors of the reduced eigenvalue problem, where the contribution of each beam mode on the POMs is identified. Although the POMs show little difference compared to the cantilever beam modes in this case, they still emerge as a superior basis for the reduced order model. Figs. 3(e) and (f) show the snapshots of the spatial response of the cantilever at various time steps obtained by the 10-d.o.f.

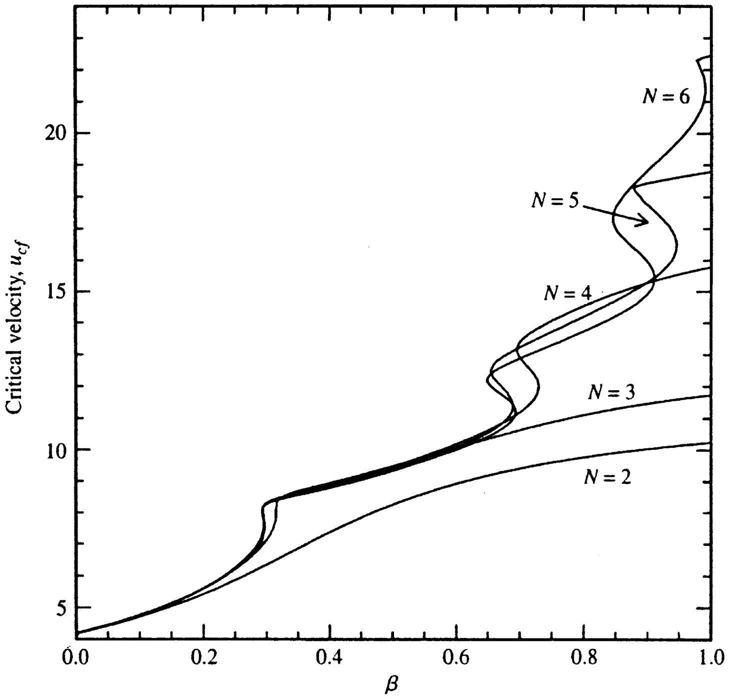

Fig. 2. The stability diagram of u_{cf} versus β for Galerkin solutions of the undamped horizontal fluid-conveying cantilever pipe with an increasing number of basis functions, N.

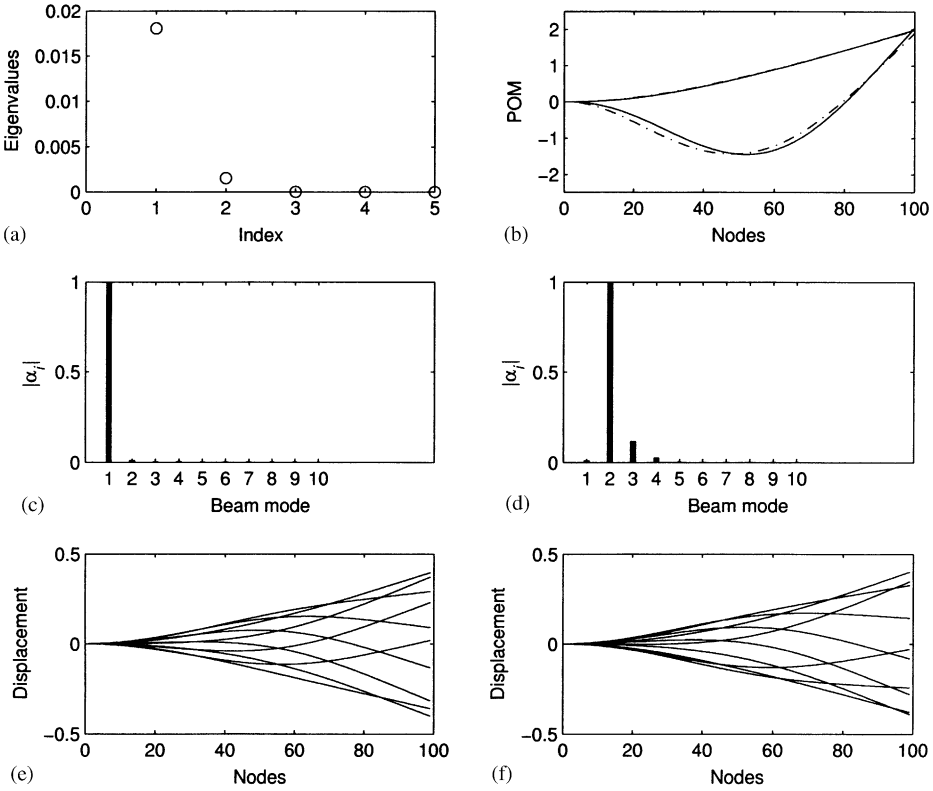

Fig. 3. The system with $\beta = 0.22$, $\alpha = 0$ and $u = 6.68$: (a) eigenvalue spectrum from *semi-analytical approach*; (b) first and second POMs (—) and cantilever beam modes (-.-.-); bar chart of (c) first eigenvector; (d) second eigenvector; temporal snapshots of spatial responses; (e) Fourier–Galerkin scheme with $N = 10$; (f) POD-Galerkin approach with $N = 2$.

Fourier–Galerkin and 2-d.o.f. POD-Galerkin method. The spatial responses obtained using these two methodologies show an excellent match, as expected. While only two POMs can adequately capture the system dynamics, four beam modes are necessary for the same purpose as seen from Figs. 3(c) and (d).

Similar results for the case of $\beta = 0.5$ with $u = 10.6$ are shown in Fig. 4. This case presents the system behaviour just after the first jump in the stability diagram in Fig. 2. The optimal dimension of the reduced order system is again two, as observed from the eigenvalue distribution of the correlation matrix in Fig. 4(a). The corresponding spatial shapes of the dominant POMs along with the corresponding normal modes are shown in Fig. 4(b). The POMs clearly exhibit noticeable differences compared to the beam modes. In this case, however, six beam modes are necessary for converged solution, as evidenced in Figs. 4(c) and (d). The spatial response profile obtained using a 2-d.o.f. POD-Galerkin and a 10-d.o.f. Fourier–Galerkin scheme exhibit good agreement as plotted in Figs. 4(e) and (f).

For $\beta = 0.6$ and flow velocity $u = 11.5$, which corresponds to the case just below the second jump in the stability diagram in Fig. 2, the results are shown in Fig. 5. Except for slightly higher contributions of the same beam modes in the POMs, the results for the eigenvalue spectrum,

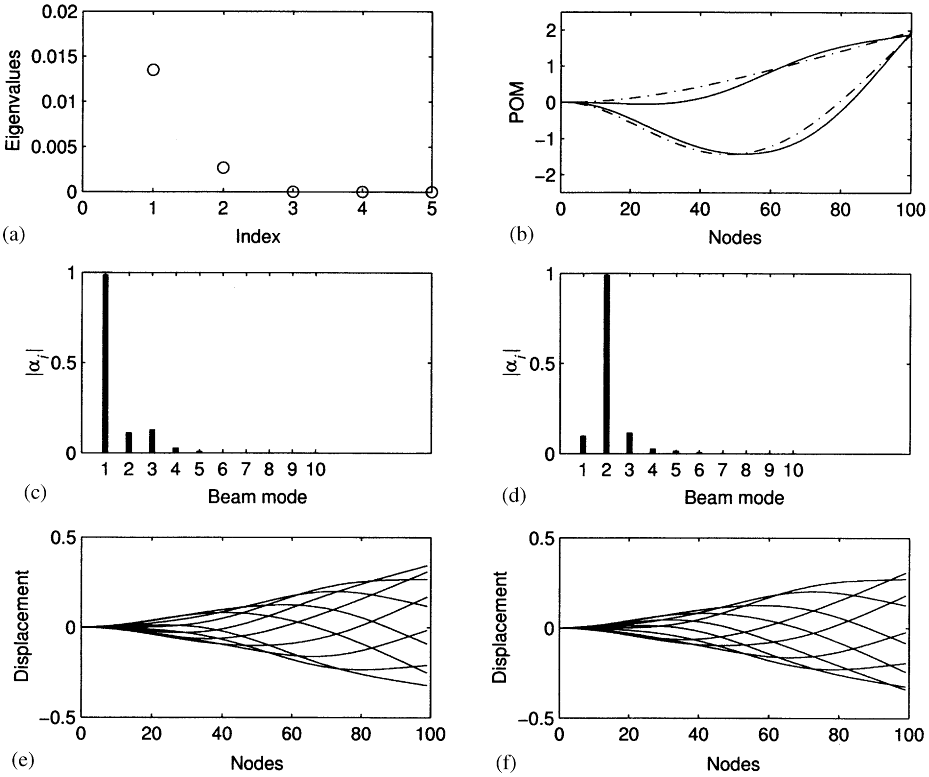

Fig. 4. The system with $\beta = 0.5$, $\alpha = 0$ and $u = 10.6$: (a) eigenvalue spectrum from *semi-analytical approach*; (b) first and second POMs (—) and cantilever beam modes (-.-.-); bar chart of (c) first eigenvector; (d) second eigenvector; temporal snapshots of spatial responses; (e) Fourier–Galerkin scheme with $N = 10$; (f) POD-Galerkin approach with $N = 2$.

POMs and corresponding response from Fourier–Galerkin and POD-Galerkin scheme differ little from those of Fig. 4, as expected.

Next, we consider the case of $\beta = 0.7$ and $u = 14.5$ (Fig. 6), corresponding to a system just after the second jump in the stability diagram (Fig. 2). As stated before, this jump is associated with the advent of a new beam mode in the Fourier–Galerkin mode. In Fig. 6(a), the eigenvalue spectrum is again dominated by two eigenvalues; the corresponding spatial profile of the POMs along with beam are plotted in Fig. 6(b). The bar charts of the corresponding eigenvectors are shown in Figs. 6(c) and (d). The associated spatial response obtained using the 10-d.o.f. Fourier–Galerkin and 2-d.o.f. POD-Galerkin schemes are shown in Figs. 6(e) and (f) which again show excellent agreement. Note that the POMs in Fig. 6(b) markedly differ from those in Fig. 5(b) depicting a case just below the second jump in the stability diagram. This phenomenon also emerges in the eigenvectors in Figs. 6(c) and (d) which display significantly enhanced contributions of the higher beam modes in comparison to the case in Figs. 5(c) and (d).

The case with $\beta = 0.82$, $\alpha = 0$ and flow velocity $u = 15.8$ (Fig. 7) presents the situation just below the third jump in the stability diagram. The eigenvalue spectrum, corresponding POMs and associated bar charts of the eigenvectors are shown in Figs. 7(a) and (d). The spatial response

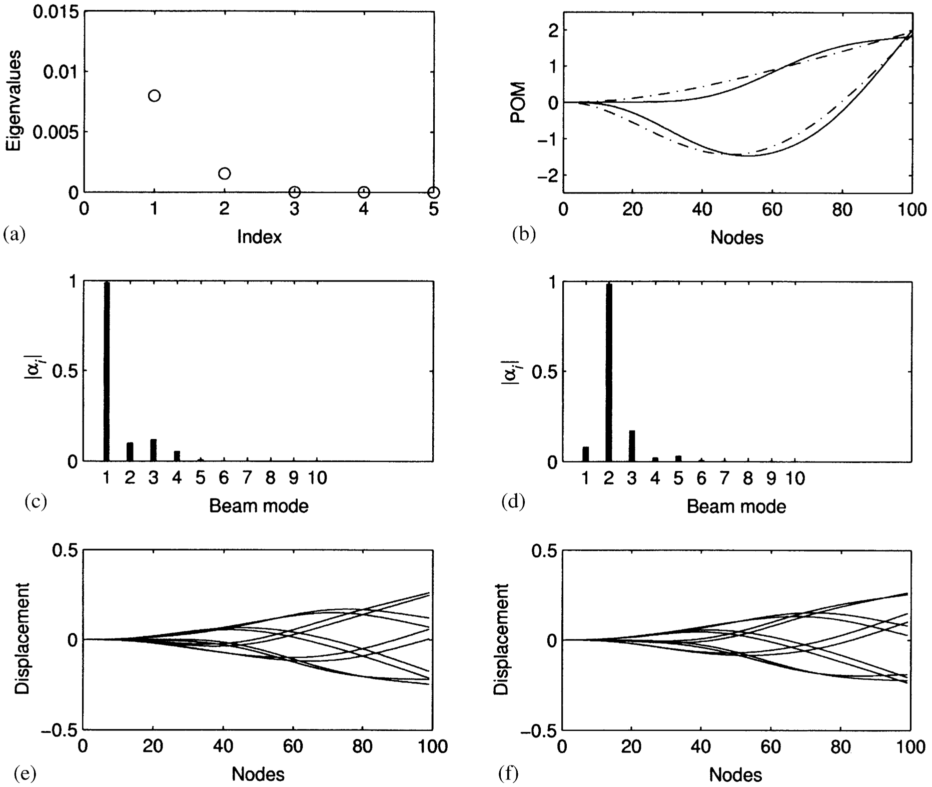

Fig. 5. The system with $\beta = 0.6$, $\alpha = 0$ and $u = 11.5$: (a) eigenvalue spectrum from *semi-analytical approach*; (b) first and second POMs (—) and cantilever beam modes (-.-.-); bar chart of (c) first eigenvector; (d) second eigenvector; temporal snapshots of spatial responses; (e) Fourier–Galerkin scheme with $N = 10$; (f) POD-Galerkin approach with $N = 2$.

profile obtained through 10-d.o.f. Fourier–Galerkin and 2-d.o.f. POD-Galerkin scheme are plotted in Figs. 7(e) and (f). Some differences between Figs. 6 and 7 can be observed. In order to study the effect of structural damping, similar results are presented in Fig. 8 with $\alpha = 10^{-2}$. The presence of damping appears to minimize the effect of higher beam modes, as observed by comparing Figs. 7(c), (d) and 8(c), (d). This effect also manifests itself through the alteration of the spatial response profile in Figs. 8(e) and (f) compared to Figs. 7(e) and (f).

Next, we consider the situation with $\beta = 0.875$ and $\alpha = 0$ (Fig. 9) just after the third and penultimate jumps in the stability diagram associated with the peculiar case where the system is restabilized after the first loss of stability and then becomes unstable again. The case with flow velocity $u = 14.85$ describes the LCO of the system after its first loss of stability shown in Fig. 2. The eigenvalue spectrum, corresponding POMs, bar charts of the eigenvectors and spatial response from the 10-d.o.f. Fourier–Galerkin and 2-d.o.f. POD-Galerkin schemes are plotted in Figs. 9(a)–(f). Similar results with $u = 17.25$ involving a LCO after the second loss of stability is shown in Fig. 10. In both cases (Figs. 9 and 10), only two dominant POM eigenvalues are present. However, a significant change in POMs is observed in Fig. 10(b) in comparison to Fig. 9(b). This aspect directly manifests itself through the rearrangement of the beam mode contributions in Figs. 10(c), (d) and 9(c), (d).

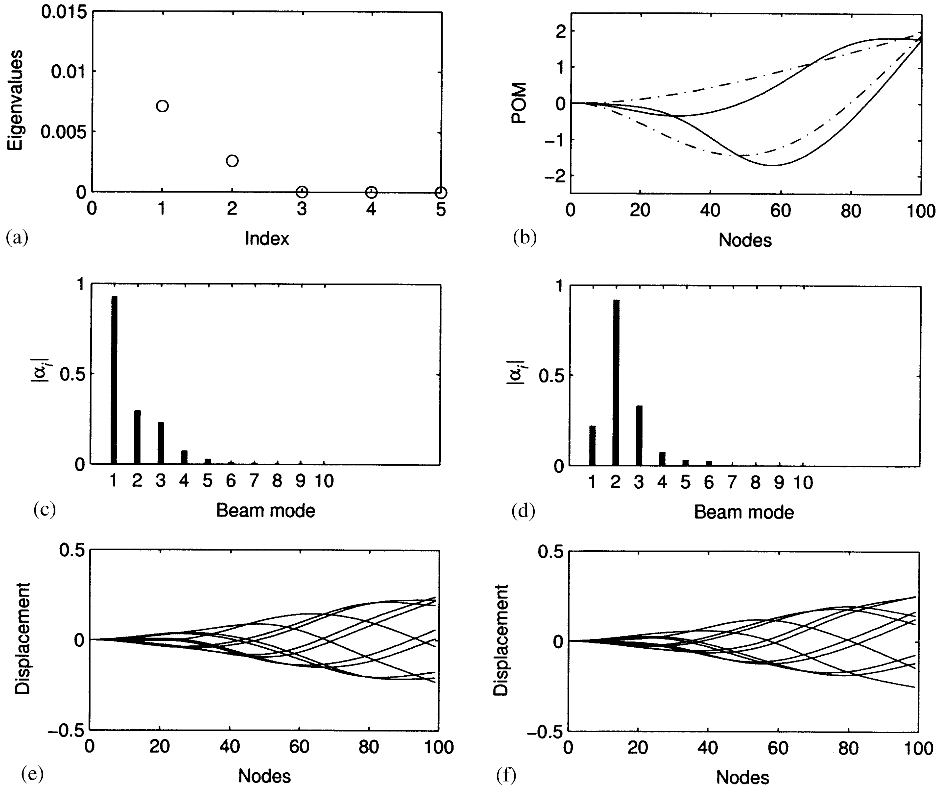

Fig. 6. The system with $\beta = 0.7$, $\alpha = 0$ and $u = 14.5$: (a) eigenvalue spectrum from *semi-analytical approach*; (b) first and second POMs (—) and cantilever beam modes (-.-.-); bar chart of (c) first eigenvector; (d) second eigenvector; temporal snapshots of spatial responses; (e) Fourier–Galerkin scheme with $N = 10$; (f) POD-Galerkin approach with $N = 2$.

The activation of an ever increasing number of cantilever beam modes with increasing β, as displayed in Figs. 3–7, 9 and 10 is summarized in Table 1. In the table, "nodes" and "antinodes" are only nominal, since, because of the travelling-wave component in the mode shape [1], they are not true nodes and antinodes. The number of modes in the diagrams (c, d) of Figs. 3–7, 9 and 10 is the total number that is found in POMs 1 and 2 that can be seen in the bar charts.

It is seen that by all three measures used in the table, there is clearly one more mode implicated after each jump, reinforcing thereby the findings in the earlier work by Semler et al. [8]. It is also noted, again in agreement with Semler et al., that when damping is added, as in Fig. 8 ($\beta = 0.82$) the number of nodes and antinodes drops to two, and the number of modes in (c, d) to only five.

6. Range of β over which POMs are effective

In the foregoing the efficacy of the proper orthogonal decomposition method was assessed *locally* (in terms of β), in the following sense. For example, to obtain the POD results for Fig. 3 ($\beta = 0.22$), the POMs were obtained from time series of the response at the same β. The same was

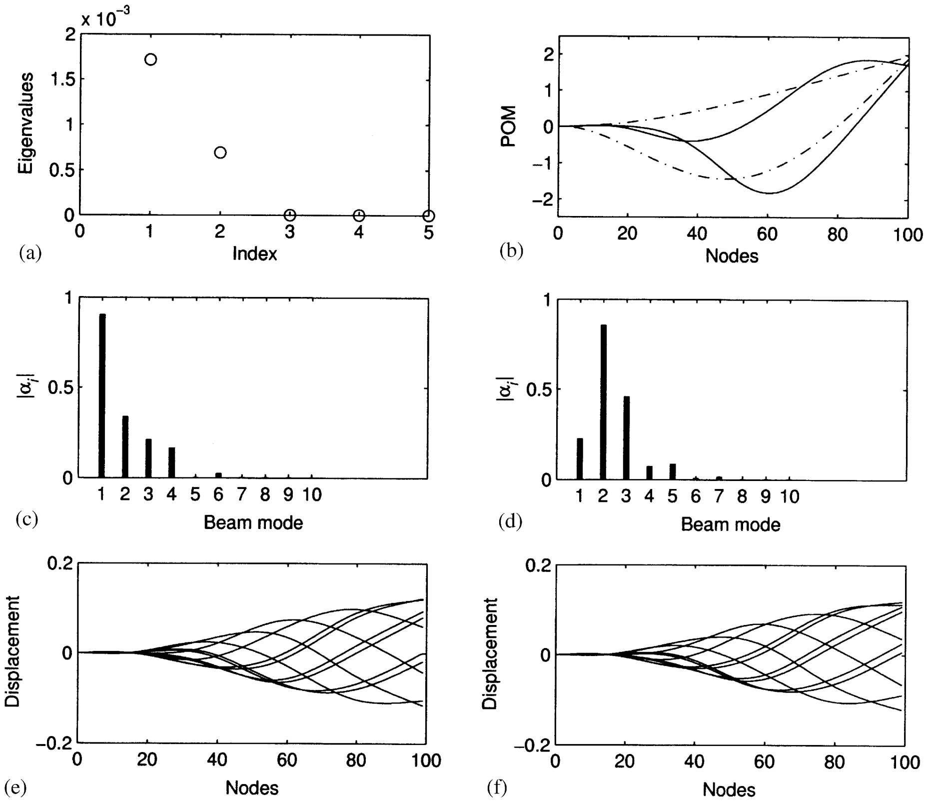

Fig. 7. The system with $\beta = 0.82$, $\alpha = 0$ and $u = 15.8$: (a) eigenvalue spectrum from *semi-analytical approach*; (b) first and second POMs (—) and cantilever beam modes (-.-.-); bar chart of (c) first eigenvector; (d) second eigenvector; temporal snapshots of spatial responses; (e) Fourier–Galerkin scheme with $N = 10$; (f) POD-Galerkin approach with $N = 2$.

Table 1
The number of beam modes involved in the mode shapes of the oscillating cantilever

Location relative to jumps	β	Number of “nodes”	Number of “antinodes”	Number of modes in the figures	Approx. u/u_{cr}
Before 1st jump	0.22	1	1	4	1.1
After 1st jump	0.5	2	2	5	1.2
Before 2nd jump	0.6	2	2	5	1.2
After 2nd jump	0.7	3	3	6	1.1
After 2nd jump	0.82	3	3	6+	1.2
Before 3rd jump	0.875	3	3	6	1.1
After 3rd jump	0.875	4	4	7	1.1

true for the results presented for each of Figs. 4–10. The efficacy of POMs obtained at one flow velocity to predict the dynamics for different flow velocities, u (but for the same values of β and γ) was tested before [6,7], and will not be commented upon in detail here—other than to say that it

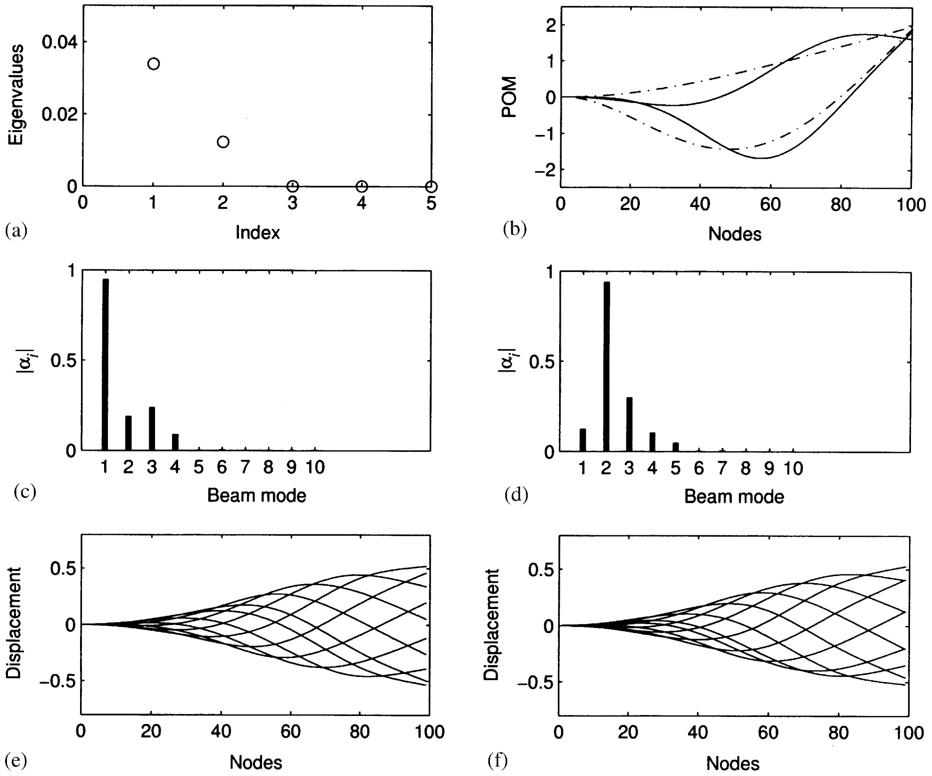

Fig. 8. The system with $\beta = 0.82$, $\alpha = 10^{-2}$ and $u = 15.8$: (a) eigenvalue spectrum from *semi-analytical approach*; (b) first and second POMs (—) and cantilever beam modes (-.-.-); bar chart of (c) first eigenvector; (d) second eigenvector; temporal snapshots of spatial responses; (e) Fourier–Galerkin scheme with $N = 10$; (f) POD-Galerkin approach with $N = 2$.

was found to be quite good, in the sense of adequately reproducing a bifurcation diagram in which u was the varied parameter, for u, say, double the value for which the POMs were constructed.

Here we have done the same type of test for varying β. By examining the results in Figs. 3–10, it is clear that the POMs change significantly as β is varied in this strongly coupled fluid–structure interaction system; thus, it was not at all clear that POMs obtained from time traces at one β would properly represent the dynamics at another β—not even being sure that the Hopf bifurcation would be captured at this other β.

Fig. 11 shows the results of this investigation.[4] It is seen in Fig. 11(b) that with POMs obtained at $\beta = 0.25$, a little below the first jump in the stability diagram, the first jump is adequately predicted. The dynamics for higher β is qualitatively reasonably well predicted, but quantitatively deteriorating with increasing β. Thus, whilst the Hopf bifurcation is predicted to occur up to $\beta \to 1$, (1) the location of the second jump is at a higher β than it

---

[4] The faint, dotted vertical lines shunting the S-shaped jumps signify that, if one were to increase β, while tracking the Hopf bifurcation point, u_{cr}, the curve would jump up discontinuously, as shown. This is also what is obtained numerically if one varies β while determining u_{cr}. If, on the other hand, one varies u while determining the equivalent β_{cr} for neutral stability, then the full S-curve is obtained.

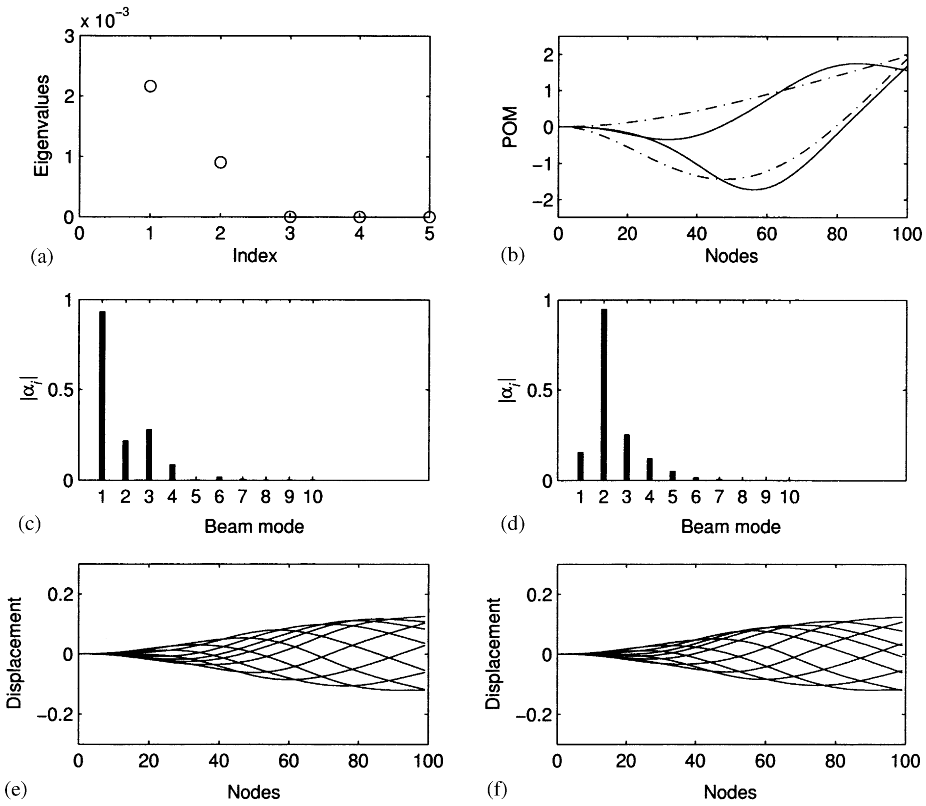

Fig. 9. The system with $\beta = 0.875$, $\alpha = 0$ and $u = 14.85$: (a) eigenvalue spectrum from *semi-analytical approach*; (b) first and second POMs (—) and cantilever beam modes (-.-.-); bar chart of (c) first eigenvector; (d) second eigenvector; temporal snapshots of spatial responses; (e) Fourier–Galerkin scheme with $N = 10$; (f) POD-Galerkin approach with $N = 2$.

should be, (2) subsequent jumps are not predicted at all, and (3) the critical values of u are underestimated.

Similarly, using POMs obtained between the first and second jumps, Fig. 11(c), this middle range of β is predicted best, but the quantitative prediction of the critical u deteriorates for the lower and higher β. Fig. 11(d) shows the results obtained with POMs from simulation *after* the second jump, and it is seen that the first jump is totally obliterated.

The conclusion is that the performance of the POD method (for POMs obtained at a specific β) as β is varied is rather mixed. This is an important conclusion, showing a much more severe limitation of the method in terms of the mass parameter β than was obtained before [6,7] in terms of the dimensionless velocity u.

7. Conclusion

A reduced order model of the non-linear PDE describing the dynamics of a horizontal cantilever conveying fluid is derived using the beam modes as well as proper orthogonal modes.

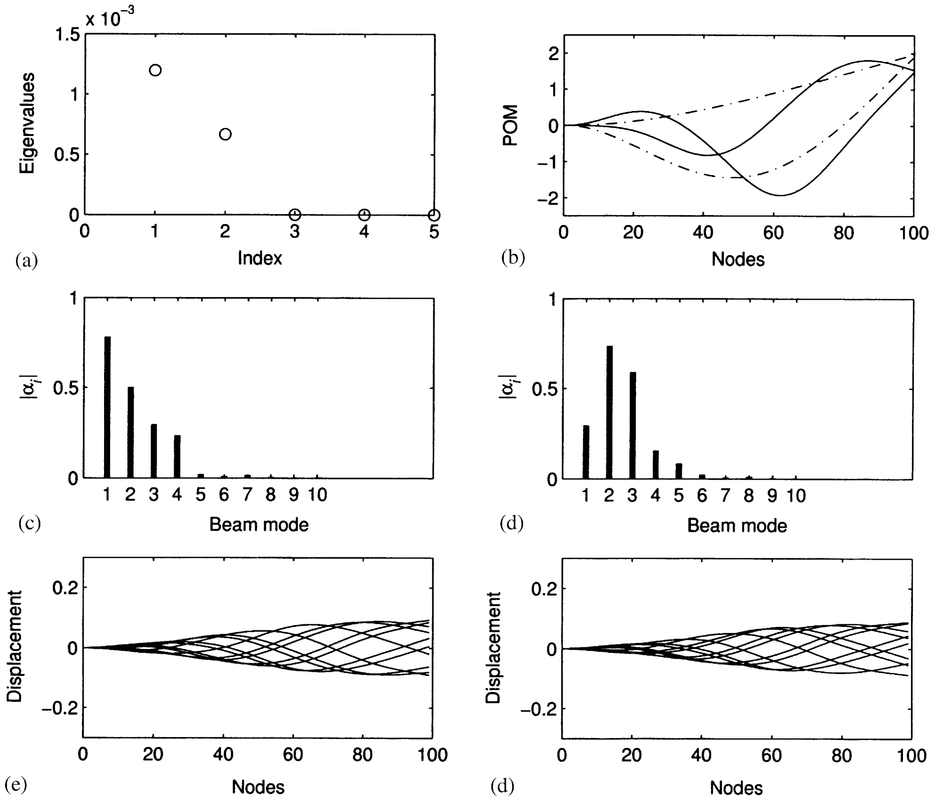

Fig. 10. The system with $\beta = 0.875$, $\alpha = 0$ and $u = 17.25$: (a) eigenvalue spectrum from *semi-analytical approach*; (b) first and second POMs (—) and cantilever beam modes (-.-.-); bar chart of (c) first eigenvector; (d) second eigenvector; temporal snapshots of spatial responses; (e) Fourier–Galerkin scheme with $N = 10$; (f) POD-Galerkin approach with $N = 2$.

The evolution of the proper orthogonal modes with respect to the variation of mass ratio reveals interesting spatial coherent structures in the post-flutter dynamics which dramatically differ from the cantilever beam modes. Depending on the mass ratio parameter, the Fourier–Galerkin scheme necessitates a progressively higher number of degrees of freedom to obtain a converged solution of the non-linear PDE describing the dynamics of the fluid-conveying tube. Focusing on the linear stability diagram, it emerges that only the 2 d.o.f. POD-Galerkin model, in contrast to the up to 10-d.o.f. Fourier–Galerkin model, can consistently capture the system behaviour irrespective of the jumps in the stability plot associated with the addition of a new beam mode in the Fourier–Galerkin scheme.

An important conclusion reached in Section 6 is that the range of β for successful quantitative prediction of the dynamics is rather limited, if the POMs are obtained at a specific β, β_s. Without having the 10 d.o.f. Fourier–Galerkin results to calibrate the system (in the sense of knowing which modes, say which beam modes, are active), prediction for β substantially higher or lower than β_s is not very good quantitatively.

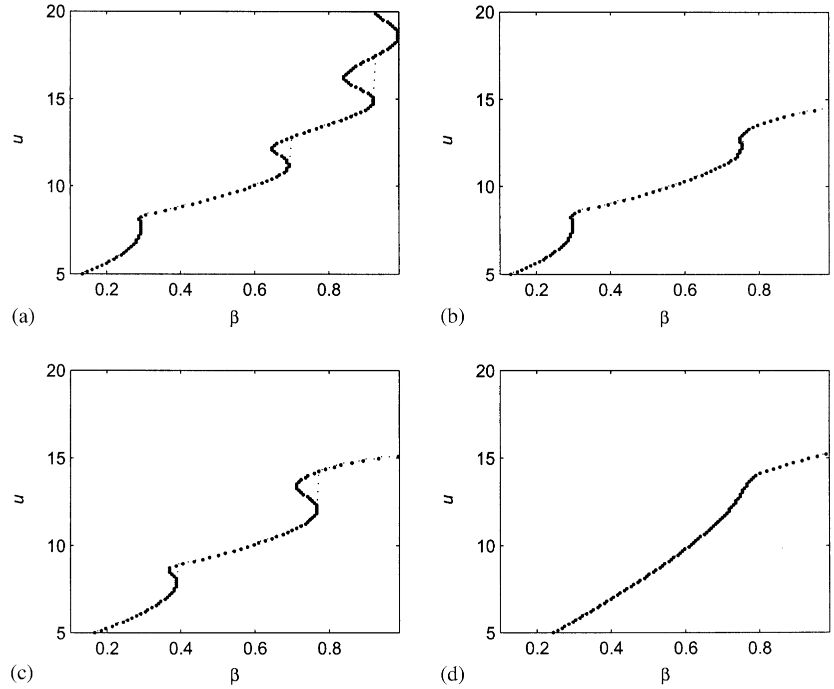

Fig. 11. (a) Stability diagram obtained by the Fourier–Galerkin method with $N = 10$. Stability diagrams with POMS obtained at (b) $\beta = 0.25$, $u = 7$; (c) $\beta = 0.5$, $u = 10.6$; (d) $\beta = 0.75$, $u = 14$; $\alpha = 0$ throughout.

Acknowledgements

The authors gratefully acknowledge the financial support of NSERC and FCAR; the second author was financially supported by a NSERC Postdoctoral Fellowship.

References

[1] M.P. Païdoussis, *Fluid–Structure Interactions: Slender Structures and Axial Flow*, Academic Press, London, 1998.

[2] M.P. Païdoussis, Dynamics of tubular cantilevers conveying fluid, *Journal of Mechanical Engineering Science* 12 (1970) 85–103.

[3] M.P. Païdoussis, G.X. Li, Pipes conveying fluid: a model dynamical problem, *Journal of Fluids and Structures* 7 (1993) 137–204.

[4] C. Semler, G.X. Li, M.P. Païdoussis, The non-linear equations of motion of pipes conveying fluid, *Journal of Sound and Vibration* 169 (1994) 577–599.

[5] C. Semler, M.P. Païdoussis, Intermittency route to chaos of a cantilevered pipe conveying fluid with a mass defect at the free end, *Journal of Applied Mechanics* 62 (1995) 903–907.

[6] A. Sarkar, M.P. Païdoussis, A cantilever conveying fluid: coherent modes versus beam modes, *International Journal of Non-Linear Mechanics* 39 (2004) 467–481.

[7] A. Sarkar, M.P. Païdoussis, A compact limit cycle oscillation (LCO) model for a cantilevered fluid-conveying pipe, *Journal of Fluids and Structures* 17 (2001) 525–539.

[8] C. Semler, H. Alighanbari, M.P. Païdoussis, A physical explanation of the destabilizing effect of damping, *American Society of Mechanical Engineers Journal of Applied Mechanics* 65 (1998) 642–648.

[9] M. Loève, *Probability Theory*, 4th Edition, Springer, New York, 1977.

[10] L. Sirovich, Turbulence and dynamics of coherent structures, part I: coherent structures, *Quarterly of Applied Mathematics* 45 (1987) 561–571.

[11] L. Sirovich, Chaotic dynamics of coherent structures, *Physica D* 37 (1989) 126–145.

[12] E.H. Dowell, K.C. Hall, M.C. Romanoski, Eigenmode analysis in unsteady aerodynamics: reduced order models, *Applied Mechanics Reviews* 50 (1997) 371–386.

[13] K.C. Hall, J.P. Thomas, E.H. Dowell, Proper orthogonal decomposition technique for transonic unsteady aerodynamic flows, *American Society of Aeronautics and Astronautics Journal* 38 (2000) 1853–1862.

[14] J.P. Cusumano, B.Y. Bai, Period-infinity periodic motions, chaos, and spatial coherence in a 10 degree of freedom impact oscillator, *Chaos, Solitons and Fractals* 3 (1993) 515–535.

[15] X. Ma, M.F.A. Azeez, A.F. Vakakis, Non-linear normal modes and non-parametric system identification of non-linear oscillators, *Mechanical Systems and Signal Processing* 14 (2000) 37–48.

[16] A. Sarkar, R. Ghanem, Mid-frequency structural dynamics with parameter uncertainty, *42nd AIAA/ASME/ASCE/ASC Structures, Structural Dynamics, and Materials Conference*, 2001, AIAA-2001-1454.

[17] M. Amabili, A. Sarkar, M.P. Païdoussis, Reduced-order models for non-linear vibrations of cylindrical shells via the proper orthogonal decomposition method, *Journal of Fluids and Structures* 18 (2003) 227–250.

[18] J.P. Cusumano, D.C. Lin, Bifurcation and modal interaction in a simplified model of bending torsion vibrations of a thin elastica, *American Society of Mechanical Engineers Journal of Vibration and Acoustics* 117 (1995) 30–42.

[19] C. Semler, W.C. Gentleman, M.P. Païdoussis, Numerical solutions of second order implicit non-linear ordinary differential equations, *Journal of Sound and Vibration* 195 (1996) 553–574.